condensed matter

MDPI

Article

Resonant Quantum Kicked Rotor as A Continuous-Time Quantum Walk

Michele Delvecchio [1], Francesco Petiziol [1,2] and Sandro Wimberger [1,2,*]

[1] Dipartimento di Scienze Matematiche, Fisiche ed Informatiche, Università di Parma, Parco Area delle Scienze 7/A, 43124 Parma, Italy; michele.delvecchio@studenti.unipr.it (M.D.); francesco.petiziol@unipr.it (F.P.)

[2] Italian National Institute for Nuclear Physics (INFN), Sezione di Milano Bicocca, Gruppo Collegato di Parma, 43124 Parma, Italy

* Correspondence: sandromarcel.wimberger@unipr.it

Received: 13 November 2019; Accepted: 8 January 2020; Published: 11 January 2020

Abstract: We analytically investigate the analogy between a standard continuous-time quantum walk in one dimension and the evolution of the quantum kicked rotor at quantum resonance conditions. We verify that the obtained probability distributions are equal for a suitable choice of the kick strength of the rotor. We further discuss how to engineer the evolution of the walk for dynamically preparing experimentally relevant states. These states are important for future applications of the atom-optics kicked rotor for the realization of ratchets and quantum search.

Keywords: atom-optics kicked rotor; quantum resonance; continuous-time quantum walks; Bose–Einstein condensates; quantum interference

1. Introduction

Generally speaking, quantum walks (QWs) are the quantum-mechanical analogue of classical random walks [1]. Whilst there is no stochastic component in QW prior to measurements, QWs are characterized by the interference of many paths in the walker's space, shaping the finally obtained probability distributions. The engineering of these distributions, or more generally of the amplitudes that result in them, may find practical applications for the creation of specific initial states. These may be useful for the implementation of quantum ratchets [2–7] and quantum search algorithms [8,9].

The first result of this paper is the interesting observation that a continuous-time quantum walk (CTQW) on the line leads to equal probability distributions in the walker's space to the momentum distributions obtained in the evolution of the quantum kicked rotor (QKR) at quantum resonance conditions. CTQWs have been realized so far with optical cavities [10], nuclear spins in magnetic fields [11], optical waveguides [12], photonic chips [13], polarization of single photons [14], and Bose–Einstein condensates in optical lattices [15]. Only recently, the experimental realization, dubbed the atom-optics kicked rotor based on (ultra)cold atoms, has been proposed as an implementation of discrete-time [16] and continuous-time [17] quantum walks in momentum space. The experimental implementation of such momentum quantum walks was largely discussed in [18,19]. Similar observations on the interference patterns in the resonant quantum kicked rotor and possible analogies with quantum walks were reported in, e.g., [20–27]. Here, we discuss their equivalence from a general viewpoint first, showing a direct connection between the Hamiltonians describing the two processes and then by studying the probability distributions explicitly for exemplary initial states. In particular, we derive the distributions resulting from the choice of initial superposition states in the momentum basis. These results are then used for discussing how to engineer interesting states by means of the

QKR/CTQW evolution. This is done by optimizing the starting state, which is typically limited to superpositions of just a few momentum eigenstates in the atom-optics implementation of the QKR [2–7,18,19,28].

The paper is structured as follows: In Section 2, we review known results for the QKR at resonance conditions, and we introduce the concept of a standard CTQW, as defined in [8]. In Section 3, we discuss the equivalence between these two models. This helps us to analyze, in Section 4, the formation of exotic interference patterns in the evolution of the walker, which can be exploited as a tool for preparing interesting states for the implementation of quantum ratchets [2–7] and the quantum search algorithm; see, e.g., [9] for a specific proposal. Finally, Section 5 summarizes our findings and provides some outlooks for further work.

2. Probability Distributions of the Walks

2.1. Review of the QKR

The quantum kicked rotor [29–31] is usually described by the rescaled dimensionless Hamiltonian:

$$\hat{\mathcal{H}} = \frac{\hat{p}^2}{2} + \kappa \cos\hat{\theta} \sum_{j=1}^{T} \delta(t - j\tau), \tag{1}$$

where p is the momentum, θ the periodic position, $\kappa > 0$ the kick strength, and τ the period of the kicks. In the following, we will assume perfect conditions for the principal quantum resonance of the kicked rotor [32], and for simplicity, we set $\tau = 4\pi$. In its atom-optics realization [6,33], the above Hamiltonian only couples momentum states that differ by a multiple of two photonic recoils so that we may separate the momentum into an integer part n and a conserved non-integer part called the quasimomentum arising from the implementation. Perfect quantum resonance occurs for zero quasimomentum for $\tau = 4\pi$, and we will neglect its impact in the sequel. Implementations of the QKR based on Bose–Einstein condensates allow one a precise control of quasimomentum with a high resolution [2–6,18,28,34,35]. Since the free evolution part

$$\hat{F} = e^{-\mathrm{i}\tau\frac{\hat{p}^2}{2}} \tag{2}$$

at quantum resonance is just equal to unity, the evolution is only given by the time-periodic kicks impacted by the one cycle Floquet operator:

$$\hat{\mathcal{U}} = e^{-\mathrm{i}\kappa\cos\hat{\theta}}. \tag{3}$$

$\hat{\theta}$ represents the angular (spatial) coordinate of the system. The evolution occurs in (angular) momentum space at discrete integers represented by the (angular) momentum operator $\hat{p} = \hat{n} = -\mathrm{i}\mathrm{d}/\mathrm{d}\theta$, with periodic (cyclic) boundary conditions. At quantum resonance, the momentum distribution of a single momentum initial state, e.g., $n_0 = 0$, expands symmetrically around its initial value and displays ballistic expansion, i.e., with a standard deviation proportional to the number of applied kicks [6,32]. Typical pictures of such momentum distributions were plotted, e.g., in [6,17].

In what follows, we review the calculation from [36] for the special case of zero quasimomentum. If we choose as the initial state the following plane wave of momentum $p_0 = n_0 \in \mathbb{Z}$:

$$\psi_{n_0}(\theta) = \frac{1}{\sqrt{2\pi}} e^{\mathrm{i}n_0\theta}, \tag{4}$$

after t kicks (or a total time t in units of τ), we have:

$$\hat{\mathcal{U}}^t = e^{-\mathrm{i}\kappa t\cos(\hat{\theta})}. \tag{5}$$

Then, the probability amplitudes in the basis of momentum states $\{|n\rangle\}_{n\in\mathbb{Z}}$ are:

$$\left\langle n\middle|\hat{\mathcal{U}}^t\psi_{n_0}\right\rangle = \int_0^{2\pi}\frac{\mathrm{d}\theta}{2\pi}e^{-\mathrm{i}\kappa t\cos(\hat{\theta})}e^{\mathrm{i}(n_0-n)\theta} = -\mathrm{i}^{n-n_0}J_{n-n_0}(\kappa t)\,, \tag{6}$$

where in the last equality, we have used the following integral representation of the Bessel function, Identity [9.1.21] from [37],

$$\frac{1}{2\pi}\int_0^{2\pi}\mathrm{d}\theta e^{\mathrm{i}z\cos(\theta)}e^{-\mathrm{i}n\theta} = \mathrm{i}^n J_n(z)\,. \tag{7}$$

Finally, the probability distribution for the momentum space evolution is found by taking the modulus squared of Equation (6), which gives:

$$P_\kappa(n,t|n_0) = |J_{n-n_0}(\kappa t)|^2\,. \tag{8}$$

From the latter equation, we will observe, in the next subsections, that the behavior of the QKR at resonance conditions is reminiscent of the one of a CTQW.

2.2. Evolution of CTQW

Following Fahri and Gutmann [38] or Portugal's book [8], we know that the evolution operator for a one-dimensional CTQW on a line is defined as:

$$\hat{U}(t) = e^{-\mathrm{i}\hat{H}_\gamma t}\,, \tag{9}$$

where the Hamiltonian $\hat{H}_\gamma$ is defined by means of the following matrix elements in the walker's computational basis $\{|m\rangle\}_{m\in\mathbb{Z}}$,

$$\langle n|\,\hat{H}_\gamma\,|m\rangle = \begin{cases} 2\gamma, & \text{if } n = m; \\ -\gamma, & \text{if } n = m\pm 1; \\ 0, & \text{otherwise;} \end{cases} \tag{10}$$

or, equivalently,

$$\hat{H}_\gamma\,|m\rangle = -\gamma\,|m-1\rangle + 2\gamma\,|m\rangle - \gamma\,|m+1\rangle\,, \tag{11}$$

with γ taken with a positive value for the convention.

3. Equivalence between Resonant QKR and CTQW

3.1. Equivalence at the Hamiltonian Level

We now derive our first result, proving the equivalence between the QKR at the resonant condition and the CTQW on general grounds. We start by observing that the QKR's evolution operator at quantum resonance of Equation (5) after t kicks can be formally interpreted as being generated by a Hamiltonian $\hat{H}_\kappa = \kappa\cos\hat{\theta}$ acting continuously for a time t. This obviously is true only when one looks at the resulting dynamics for integer t, i.e., when the kick occurs. Rewriting the potential in Equation (1) $\cos(\hat{\theta}) = 1/2(\exp(\mathrm{i}\hat{\theta}) + \exp(-\mathrm{i}\hat{\theta}))$, the similarity with the nearest-neighbor couplings of the CTQW

in Equation (10) becomes quite evident. On the basis of momentum eigenstates, the Hamiltonian $\hat{H}_\kappa$ has matrix elements:

$$\begin{aligned}\langle m|\,\hat{H}_\kappa\,|n\rangle &= \int_0^{2\pi} \frac{e^{-\mathrm{i}m\theta}}{\sqrt{2\pi}}\kappa\cos\theta\frac{e^{\mathrm{i}n\theta}}{\sqrt{2\pi}}d\theta,\\ &= \begin{cases}\kappa/2 & \text{if } m = n\pm 1\\ 0 & \text{otherwise}\end{cases}.\end{aligned} \tag{12}$$

Comparing Equations (10) and (12), we thus see that, if we choose $\kappa = 2\gamma$, the following relation holds for the CTQW Hamiltonian $\hat{H}_\gamma$ and the "effective" kick Hamiltonian $\hat{H}_\kappa$ at integer t:

$$\hat{H}_\gamma = 2\gamma\mathbb{I} - \hat{H}_\kappa, \tag{13}$$

where $\mathbb{I}$ is the identity matrix over the whole walker's space. Let us now focus on the probability of being in the n^{th} momentum eigenstate, given whatever initial state $|\Psi_0\rangle$ after t kicks of our QKR,

$$P_\kappa(n,t) = \left|\langle n|\,\hat{\mathcal{U}}^t\,|\Psi_0\rangle\right|^2 = |\langle n|\,e^{-\mathrm{i}\hat{H}_\kappa t}\,|\Psi_0\rangle\,|^2\,. \tag{14}$$

The probability $P_\gamma(n,t)$ that the CTQW starting from the same state leads to the same momentum eigenstate is then, for $\gamma = \kappa/2$ and using Equations (13) and (14),

$$P_\gamma(n,t) = |\langle n|\,e^{-\mathrm{i}\hat{H}_\gamma t}\,|\Psi_0\rangle\,|^2, \tag{15a}$$
$$= |\langle n|\,e^{-\mathrm{i}(2\gamma\mathbb{I}-\hat{H}_\kappa)t}\,|\Psi_0\rangle\,|^2, \tag{15b}$$
$$= |\langle n|\,e^{-2\mathrm{i}\gamma t}e^{\mathrm{i}\hat{H}_\kappa t}\,|\Psi_0\rangle\,|^2, \tag{15c}$$
$$= |\langle n|\,e^{\mathrm{i}\hat{H}_\kappa t}\,|\Psi_0\rangle\,|^2, \tag{15d}$$
$$= P_\kappa(n,-t). \tag{15e}$$

Therefore, choosing $\gamma = \kappa/2$ produces a CTQW with a time-reversed probability distribution with respect to the evolution induced by the QKR, independent of the initial condition.

If $\kappa = -2\gamma$ is chosen instead, the two probability distributions would be equal. One can also evaluate explicitly the probability distribution of the Hamiltonian (10) using techniques from the theory of quantum walks [8]. These calculations are reported in Appendix A.

We proved that the probability distribution of a CTQW, $P_\gamma(n,t)$, is equal to the one of the QKR at resonance, $P_\kappa(n,t)$, if one chooses $\kappa = -2\gamma$. Therefore, the simple QKR at principal resonance conditions directly implements a CTQW as defined in [8]. Previously, this identity was not highlighted explicitly or was only thought to be true approximately; see the discussions in [17] and around Figure 2 in [19].

3.2. Distributions for Specific Initial States

In general, if the initial condition is $|\psi(0)\rangle$, where $|\psi(0)\rangle$ is the eigenstate with $n_0 = 0$, the state at time t is:

$$|\psi(t)\rangle = \hat{U}(t)\,|\psi(0)\rangle\,, \tag{16}$$

and the probability distribution over the walker's space is:

$$P_\gamma(m,t) = |\langle m|\psi(t)\rangle|^2\,. \tag{17}$$

From the previous Sections 2.1 and 3.1, we know that:

$$P_\gamma(m,t) = |J_m(2\gamma t)|^2\,. \tag{18}$$

We now extend the analogy between the QKR and CTQWs to an initial state consisting of a more complex superposition state of the walker's basis in Section 4. This is motivated by the idea of exploiting the evolution produced by the QKR/CTQW for preparing interesting states. The distributions after some iterations of the QKR at resonance conditions, or equivalently of a CTQW on the line, show interesting interference patterns, which can be controlled by the relative phases in the initial states. This allows us, for instance, to switch from broader final distributions to more localized ones, or from symmetric to asymmetric ones in the walker's space. We will discuss this phenomena in detail in the next Section 4.

Let us consider a generic initial state, which is described by the vector of coefficients C_n, e.g.,

$$\psi(t=0) = \mathcal{N} \begin{pmatrix} \vdots \\ C_{-2} \\ C_{-1} \\ C_0 \\ C_1 \\ C_2 \\ \vdots \end{pmatrix}, \tag{19}$$

where $\mathcal{N}$ is the normalization constant, in order to extend the theory for an initial state given by a superposition of eigenstates. The coefficients C_n are chosen to be pure phases, that is they are complex coefficients of modulus one, in order to have $\psi(t=0)$ uniformly distributed over the walker's space. Because of the freedom in choosing the global phase of the wave vector, (at least) one of the coefficients could be set equal to one. For illustrative purposes and in order to keep the discussion transparent, we consider a flat distribution over three states, thus taking $C_{-1}, C_0, C_1 \neq 0$ only. Further generalization to arbitrarily broad initial states seems obvious. Such states with more than one coefficient different from zero, but nevertheless localized in some region of the walker's space are actually more interesting for the creation of the interference profiles presented in Section 4.

The chosen initial state $\psi_0 \equiv \psi(t=0)$ is of the form:

$$\psi_0(\theta) = \frac{1}{\sqrt{3}} \frac{1}{\sqrt{2\pi}} \left(C_{-1} e^{-\mathrm{i}\theta} + C_0 + C_1 e^{\mathrm{i}\theta} \right), \tag{20}$$

where we have the three components respectively with $n_0 = -1, n_0 = 0, n_0 = 1$. Now, we use it as the initial state in order to arrive at the probability amplitude:

$$\left\langle n \middle| \hat{\mathcal{U}}^t \psi_0 \right\rangle = \frac{1}{\sqrt{3}} \int_0^{2\pi} \frac{\mathrm{d}\theta}{2\pi} e^{-\mathrm{i}n\theta - \mathrm{i}\kappa t \cos(\hat{\theta})} \left(C_{-1} e^{-\mathrm{i}\theta} + C_0 + C_1 e^{\mathrm{i}\theta} \right). \tag{21}$$

Solving the integral in the same way we do in Section 2.1, we obtain a sum of Bessel functions:

$$\left\langle n \middle| \hat{\mathcal{U}}^t \psi_0 \right\rangle = \frac{1}{\sqrt{3}} \left[C_0 J_n(\kappa t) + \mathrm{i} \left(C_1 J_{n-1}(\kappa t) - C_{-1} J_{n+1}(\kappa t) \right) \right]. \tag{22}$$

Therefore, the distribution is:

$$\begin{aligned} P_\kappa(n,t) = & \frac{1}{3} \{ |C_0|^2 J_n^2(\kappa t) + |C_1|^2 J_{n-1}^2(\kappa t) + |C_{-1}|^2 J_{n+1}^2(\kappa t) - 2\mathrm{Im}[C_0^* C_1] J_n(\kappa t) J_{n-1}(\kappa t) \\ & + 2\mathrm{Im}[C_0^* C_{-1}] J_n(\kappa t) J_{n+1}(\kappa t) - 2\mathrm{Re}\,[C_{-1}^* C_1] J_{n-1}(\kappa t) J_{n+1}(\kappa t) \}. \end{aligned} \tag{23}$$

Remembering that the coefficients are chosen with modulus equal to one, we finally have:

$$\begin{aligned} P_\kappa(n,t) = & \frac{1}{3} \{ J_n^2(\kappa t) + J_{n-1}^2(\kappa t) + J_{n+1}^2(\kappa t) - 2\mathrm{Im}[C_0^* C_1] J_n(\kappa t) J_{n-1}(\kappa t) \\ & + 2\mathrm{Im}[C_0^* C_{-1}] J_n(\kappa t) J_{n+1}(\kappa t) - 2\mathrm{Re}\,[C_{-1}^* C_1] J_{n-1}(\kappa t) J_{n+1}(\kappa t) \}. \end{aligned} \tag{24}$$

This last equation is the general form of the probability density function for an initial state given by a superposition of any three neighboring walker's states. Fixing $C_0 = 1$ by the choice of the global phase of the wavefunction and writing $C_1 = e^{i\varphi_1}$ and $C_{-1} = e^{i\varphi_{-1}}$, Equation (24) becomes:

$$\begin{aligned} P_\kappa(n,t) = \frac{1}{3}\{ & J_n^2(\kappa t) + J_{n-1}^2(\kappa t) + J_{n+1}^2(\kappa t) - 2\sin(\varphi_1) J_n(\kappa t) J_{n-1}(\kappa t) \\ & + 2\sin(\varphi_{-1})] J_n(\kappa t) J_{n+1}(\kappa t) - 2\mathrm{Re}\ \cos(\varphi_1 - \varphi_{-1}) J_{n-1}(\kappa t) J_{n+1}(\kappa t)\} . \end{aligned} \tag{25}$$

From the latter expression, the role of the phases of the coefficients is more explicitly stressed. In Section 4, we will see how this probability distribution changes by choosing different values for the respective coefficients.

In the same way, we can evaluate the distribution of the CTQW obtaining:

$$\begin{aligned} P_\gamma(n,t) = \frac{1}{3}\{ & J_n^2(2\gamma t) + J_{n-1}^2(2\gamma t) + J_{n+1}^2(2\gamma t) + 2\mathrm{Im}[C_0^* C_1] J_n(2\gamma t) J_{n-1}(2\gamma t) \\ & - 2\mathrm{Im}[C_0^* C_{-1}] J_n(2\gamma t) J_{n+1}(2\gamma t) - 2\mathrm{Re}\ [C_{-1}^* C_1] J_{n-1}(2\gamma t) J_{n+1}(2\gamma t)\} . \end{aligned} \tag{26}$$

This distribution is very similar to Equation (24) except for a phase of π in the fourth and the fifth term. This is related to the fact that we have chosen $\kappa = 2\gamma$, which, as explained in Section 3, produces a reversed-time CTQW. As a result, a biased, asymmetric walk will take the opposite direction with respect to the one in Figure 2. One can restore exact equivalence, for instance, by adding a phase of π to the prefactor C_0 or by implementing kicks with a negative strength $\kappa = -2\gamma$. This can be experimentally implemented in setups with cold atoms as in [18,19], for instance. Indeed, in that case, κ is proportional to the squared Rabi frequency and to the duration of the kick pulse, which are positive, but inversely proportional to the detuning from the atomic transition, which can have also a negative value; please see the proposal of [16] for details.

4. Engineering the Final Walk Distributions

For applications in quantum search, the typical initial distribution is not localized as studied in the previous section, but uniformly extended over the walker's space (see, e.g., [8]), or at least flat over some interval of walker states (see, e.g., a search proposal for a quantum rotor subject to two different kicking potentials in [39]). We numerically simulated QKR evolutions to verify our theoretical predictions from the previous sections. Since we proved the equivalence between the CTQW and the QKR in the previous sections, we drop from now on the corresponding labels in the probability distribution, calling it simply $P(n,t)$. In the numerical evolution, we can easily invert the evolution to produce figures that nicely illustrate the dynamics, just as done in the experiment; see [18], in particular Figure 2 therein. The backward evolution is obtained by applying the adjoint operator $\left(\hat{\mathcal{U}}^t\right)^\dagger$ after half of the total steps, i.e., after 15 kicks in our cases.

Figures 1 and 2 show some examples with different choices of the coefficients C_n. In particular, for the first plot, we chose $C_1 = C_{-1} = C_0 = 1$ and $C_n = 0$ for any $n \neq \pm 1, 0$. The evolution depicted in Figure 1a exhibits strong interference between neighboring momentum states, so we lose the usual shape of a CTQW characterized by a ballistic behavior of the peaks [8]. Analytically, using Equation (24), which is seen from the formula:

$$P(n,t) = \frac{1}{3}[J_n^2(\kappa t) + (J_{n-1}(\kappa t) - J_{n+1}(\kappa t))^2] . \tag{27}$$

Because of the parity properties of the Bessel functions, the two quadratic terms combine during the entire walk so as to suppress the external peaks. This leads to a strong interference of the participating momentum states.

The evolution shown in Figure 1c,d is obtained by rotating the phase of either C_{-1} or C_1 by π. Both cases lead to the same probability distribution,

$$P(n,t) = \frac{1}{3}[J_n^2(\kappa t) + (J_{n-1}(\kappa t) + J_{n+1}(\kappa t))^2], \qquad \text{Figure 1c,d} \tag{28}$$

since $P(n,t)$ for real coefficients only depends on their relative phase; see Equation (25).

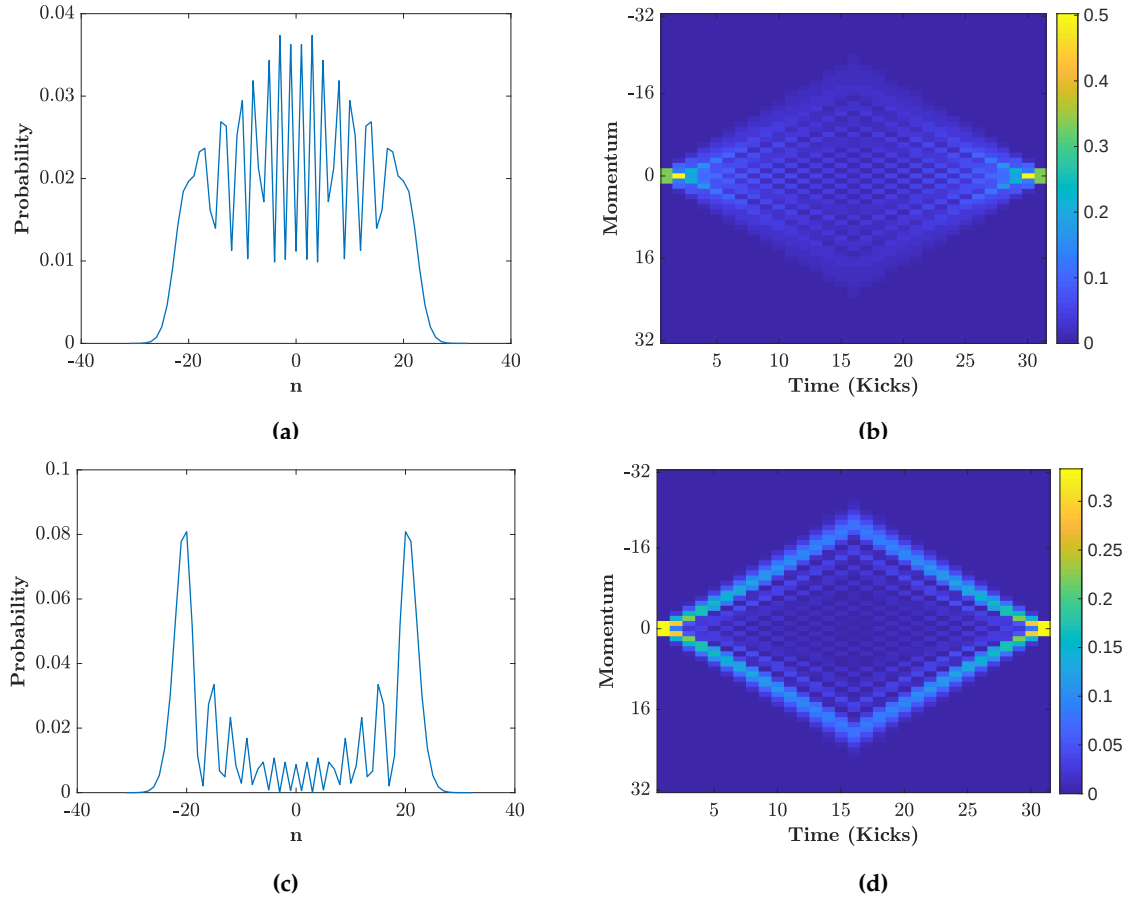

Figure 1. Probability distribution vs. momentum n after 15 kicks (**a**,**c**) and a false-color plot showing the entire evolution backward and forward in time, with inversion after 15 steps (**b**,**d**), for the initial state with coefficients $(\cdots 0,1,1,1,0\cdots)$ in (a,b) and $(\cdots 0,1,1,-1,0\cdots)$ in (c,d), centered around zero momentum. The simulations have been performed using $\kappa = 3/2$ for the quantum kicked rotor (QKR), or equivalently $\gamma = 3/4$ for the continuous-time quantum walk (CTQW).

Figure 2 shows that changing the phases of C_{-1} or C_1 by $\pi/2$ (rather than π) leads to an asymmetric walk. In fact, the two probability distributions are, respectively,

$$P(n,t) = \frac{1}{3}[(J_n(\kappa t) + J_{n+1}(\kappa t))^2 + J_{n-1}^2(\kappa t)] \qquad \text{Figure 2a,b,} \tag{29}$$

$$P(n,t) = \frac{1}{3}[(J_n(\kappa t) - J_{n-1}(\kappa t))^2 + J_{n+1}^2(\kappa t)] \qquad \text{Figure 2c,d.} \tag{30}$$

Now, the distributions are different. The parity properties of the Bessel functions induce in this case a suppression of only one side of the walk.

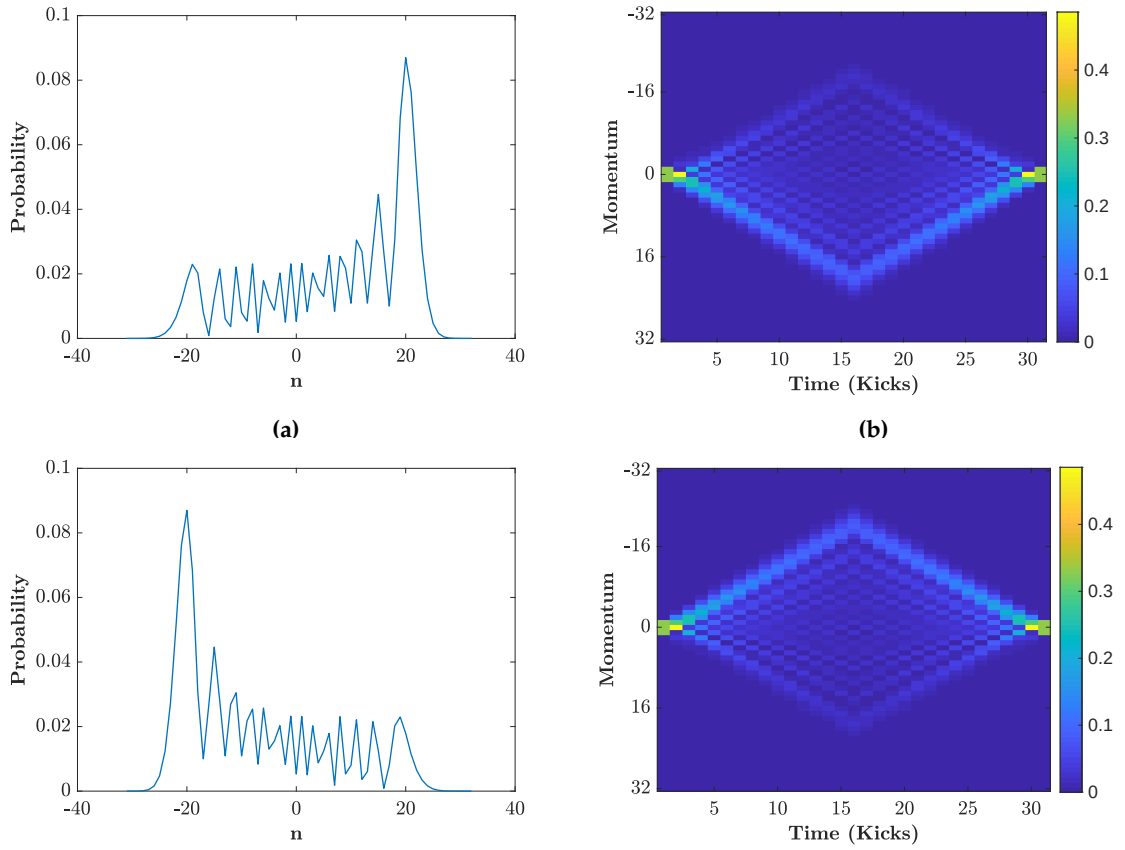

Figure 2. Same as in the previous figure, but for the initial states with coefficients centered around $n = 0$: (**a**,**b**) $(\cdots 0, \mathrm{i}, 1, 1, 0 \cdots)$; (**c**,**d**) $(\cdots 0, 1, 1, \mathrm{i}, 0 \cdots)$.

Moreover, for illustrative purposes, we look at an initial state composed of five nonzero momentum classes:

$$\psi_\beta(\theta) = \frac{1}{\sqrt{5}} \frac{1}{\sqrt{2\pi}} \left(C_{-2} e^{-\mathrm{i}2\theta} + C_{-1} e^{-\mathrm{i}\theta} + C_0 + C_1 e^{\mathrm{i}\theta} + C_2 e^{\mathrm{i}2\theta} \right) . \tag{31}$$

The procedure to calculate the final distribution is exactly the same as above. The only difference is that, in this case, we will have more interference generated by more participating neighboring momentum states, already early in the evolution. Figure 3 shows an exemplary distribution for an initial superposition with the coefficients $C_2 = C_{-2} = C_{-1} = C_0 = 1$, $C_1 = -1$, and $C_n = 0$ for any other n. We can still distinguish the two peaks at the edges seen in the case of Figure 1c, but they are just half as high as the peaks there. This difference of probability has moved towards the center where we can see now much stronger constructive interference than before.

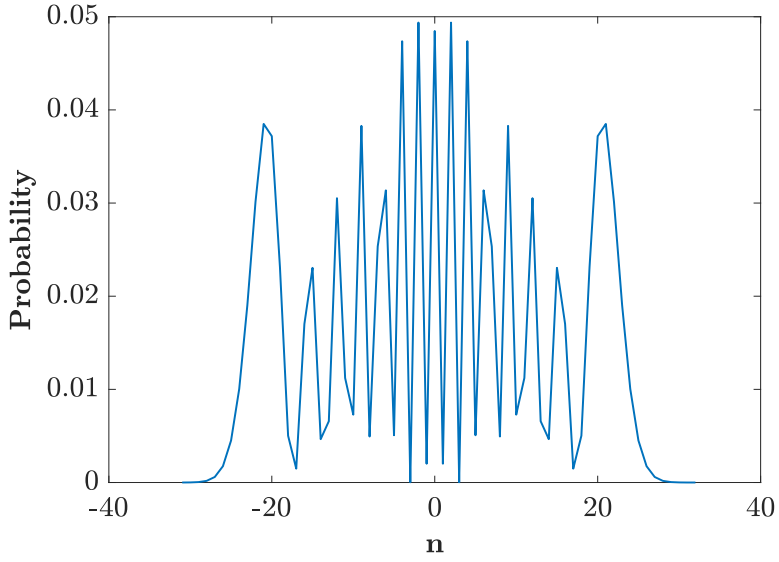

Figure 3. Distribution vs. momentum after 15 kicks with $\kappa = 3/2$, or equivalently with $\gamma = 3/4$, for the initial state with coefficients centered around $|0\rangle$: $(\cdots 0, 1, 1, 1, -1, 1, 0 \cdots)$.

All the above examples illustrate the rich dynamical behavior governed by the interference of the participating initial states and the dynamically coupled additional states of the walker's basis. Our examples already showed that the CTQW, or the equivalent QKR evolution at resonance, can be steered, biased towards one direction, and be made more localized or broader depending only on the specific choice of the initial state.

As our last example, we show how the coefficients in the initial state can be optimized in order to obtain a target distribution after a given number t of kicks. In particular, we aim at preparing a uniform distribution over N basis states, given that a generic superposition of only a few states can be experimentally realized as the input state [5,7,18,19]. The obtained distributions are of particular relevance for realizing a quantum search protocol; see, e.g., the proposals in [9,39]. For this purpose, denoting with $\boldsymbol{C} = \{C_{-1}, C_0, C_1\}$ the initial coefficients, we define a cost function $\mathcal{E}(\boldsymbol{C})$ as:

$$\mathcal{E}(\boldsymbol{C}) = \sum_{n=-N/2}^{N/2} [P(n, t; \boldsymbol{C}) - u_N]^2 , \tag{32}$$

where $P(n, t; \boldsymbol{C})$ is the walker's distribution given initial coefficients $\boldsymbol{C}$ and $u_N = \frac{1}{N}$ is the value of the target uniform distribution over N states. Given this setup, we then find numerically the coefficients $\boldsymbol{C}$ such that $\mathcal{E}(\boldsymbol{C})$ is minimal. For a given number of kicks t, the width N of the distribution is numerically probed beforehand, but we actually know that the maximal width after t kicks can be estimated to be $N \approx \pi\kappa t$, at least when starting at zero momentum only, as discussed in detail in [36]. Figure 4 shows the distributions resulting from the optimization done with parameter $\kappa = 3/2$ ($\gamma = 3/4$). In particular, Figure 4d is the distribution obtained, using Equation (24) as the walker's distribution, for the initial state with three non-zero coefficients centered around zero momentum; whereas Figure 4a–c represent the distribution for an initial state with four nonzero coefficients. In detail, Figure 4 shows the final distribution after $t = 10$ for the optimization parameter $N = 36$ (Figure 4a), $t = 15$ for $N = 52$ (Figure 4b) as used also in Figure 4d, and $t = 30$ for $N = 102$ (Figure 4c). As can be seen, we can engineer the final distribution and in particular its width by the choice of the initial coefficients, the coupling parameter κ (2γ), and the number of evolution steps. A specific experimental proposal was given in [9], where a broad distribution was first prepared along the lines above and then used for implementing a search algorithm based on our CTQW in momentum space.

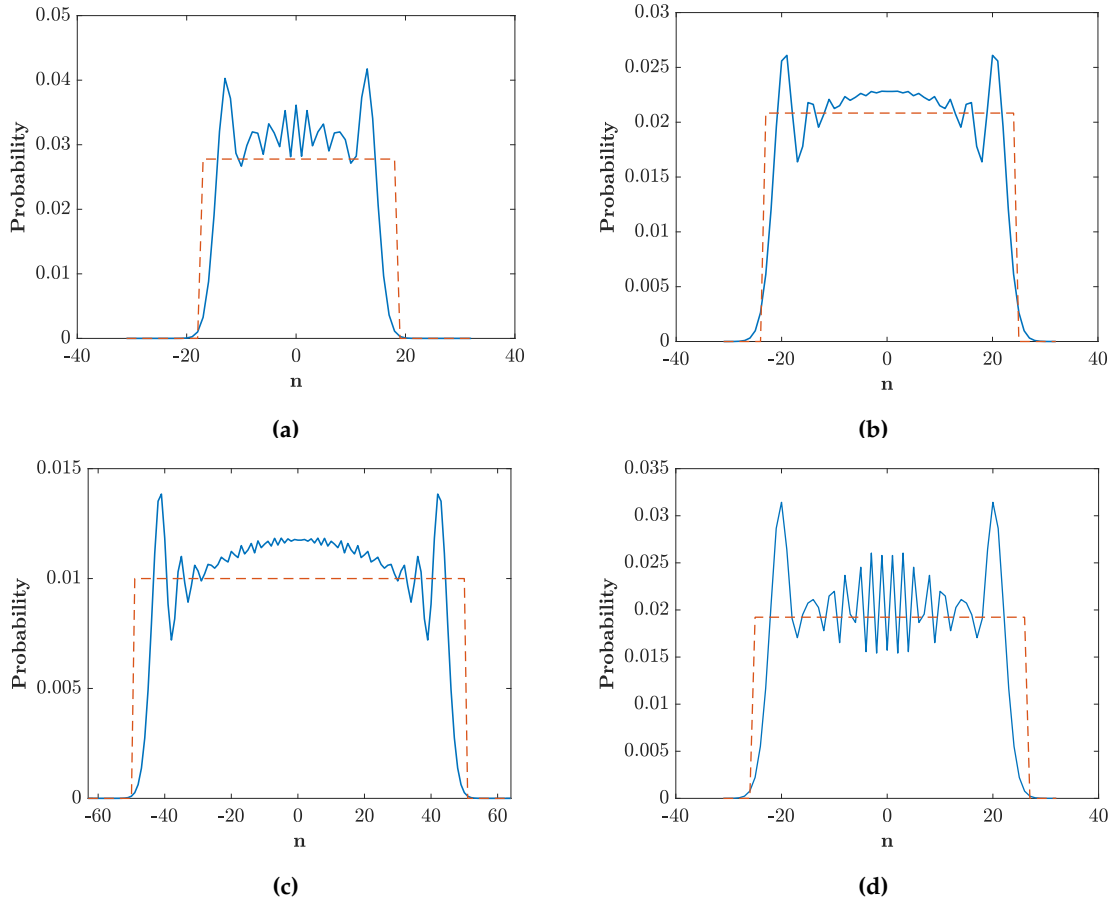

Figure 4. Probability distribution vs. momentum after a certain amount of kicks (solid line) for an initial state chosen to be spread over four states: **(a)** $(C_{-1}, C_0, C_1, C_2) = (0.40, 0.75, 0.52, 0.06)$ at $t = 10$, **(b)** $(C_{-1}, C_0, C_1, C_2) = (0.23, 0.67, 0.67, 0.23)$ at $t = 15$, **(c)** $(C_{-1}, C_0, C_1, C_2) = (0.26, 0.68, 0.68, 0.26)$ at $t = 30$, and finally, **(d)** over three states with $(C_{-1}, C_0, C_1) = (0.48, 0.73, 0.48)$ at $t = 15$. The coefficients of these initial states are engineered in order to produce a distribution close to a uniform one (dashed line) through the optimization procedure exposed in the last part of Section 4. The kick strength used is $\kappa = 3/2$ or, equivalently, $\gamma = 3/4$.

5. Conclusions and Outlook

In summary, we revisited in detail the analogy of the continuous-time quantum walk (CTQW) in momentum space and the quantum kicked rotor (QKR). This system can be realized with Bose–Einstein condensates, allowing for the necessary control over the initial conditions [2–7,18,19,28]. The typical evolution of a single initial state in the walker's space, in our case momentum space, was extended to initial states being a superposition of a few states. The resulting final distributions may be relevant for the implementation of quantum ratchets [2–7], quantum search protocols based on momentum-space CTWQs [9], as well as for the dynamical creation of interesting interference patterns in general. We see our work as a bridge between both scientific communities, working with CTQWs and QKRs, respectively, with a large potential overlap for future developments.

Interesting extensions would be the inclusion of atom–atom interactions and the investigation of higher dimensional walks. Whilst, in the experimental realization of a CTQW with a Bose–Einstein condensates expanding in an optical lattice [15], the walk occurred with interactions local in the walker's (real) space, in our CTQW, such contact interactions in real space typical for ultracold atoms would be long range in momentum space, an aspect discussed briefly in [40]. For the QKR, an effective higher dimensionality can be obtained by the application of several incommensurable kicking potentials; see [19] for a comprehensive discussion of such a possibility. Whether the analogy

between the resonant QKR and the CTQW will extend to higher dimensional walks in various geometries, with enlarged possibilities of interference between the different directions, will be the subject of future work. Furthermore, for discrete-time quantum walks with an additional coin degree of freedom, one may study the preparation of topological states and their properties; see, e.g., [41–45]. In particular, the work in [45] investigated the possibility of realizing topological phases in a double kicked QKR experiment. Mixing our state preparation scenario discussed here with the additional coin degree of freedom would thus be another interesting goal to pursue.

Author Contributions: Project design: F.P. and S.W.; numerical simulations: M.D.; analytical derivations: M.D. and F.P.; all authors contributed to the writing of the manuscript. All authors have read and agreed to the published version of the manuscript.

Funding: This research received no external funding.

Acknowledgments: We thank Renato Portugal for hints on the proof presented in Appendix A and Gil Summy and Mark Sadgrove for many useful discussions on the experimental realization.

Conflicts of Interest: The authors declare no conflict of interest.

Appendix A. Explicit Calculations for the Distributions of CTQW

We calculate explicitly the distribution of the CTQW for the system initialized in the zero-momentum state $|0\rangle$. Our results eventually show that the rather lengthy proof for the CTQW presented here can be substituted by the simpler derivation based on the QKR at resonance in Section 2.1, together with the generalization for arbitrary initial states in Section 3. We, however, show this Appendix deliberately in order to use both the languages of the CTQW and of the quantum dynamical systems (or QKR) community. We remark that the proof given here follows closely an unsolved problem in Protugal's book [8], Exercise No. 3.12.

First of all, we show by induction that the matrix $\hat{H}_\gamma$ of the CTQW on the line obeys the relation:

$$\hat{H}_\gamma^t |0\rangle = \gamma^t \sum_{n=-t}^{t} (-1)^n \binom{2t}{t-n} |n\rangle . \tag{A1}$$

This relation is indeed true for $t = 1$,

$$\hat{H}_\gamma |0\rangle = \gamma \sum_{n=-1}^{1} (-1)^n \binom{2}{1-n} |n\rangle = -\gamma |-1\rangle + 2\gamma |0\rangle - \gamma |1\rangle . \tag{A2}$$

Assuming that Equation (A1) holds for a generic t, let us prove the relation for $t+1$.

$$\begin{aligned} \hat{H}_\gamma^{t+1} |0\rangle = \hat{H}_\gamma \hat{H}_\gamma^t |0\rangle = \hat{H}_\gamma \left(\gamma^t \sum_{n=-t}^{t} (-1)^n \binom{2t}{t-n} |n\rangle \right) = \\ = -\gamma \left(\gamma^t \sum_{n=-t}^{t} (-1)^n \binom{2t}{t-n} |n-1\rangle \right) + 2\gamma \left(\gamma^t \sum_{n=-t}^{t} (-1)^n \binom{2t}{t-n} |n\rangle \right) \\ - \gamma \left(\gamma^t \sum_{n=-t}^{t} (-1)^n \binom{2t}{t-n} |n+1\rangle \right) . \end{aligned} \tag{A3}$$

Now, we change the variable $k = n - 1$ in the first term, $k = n$ in the second, and $k = n + 1$ in the third. Therefore, we arrive at:

$$\begin{aligned} \hat{H}_\gamma^{t+1} |0\rangle = \gamma^{t+1} \Bigg[- \sum_{k=-t-1}^{t-1} (-1)^{k+1} \binom{2t}{t-k-1} + 2 \sum_{k=-t}^{t} (-1)^k \binom{2t}{t-k} \\ - \sum_{k=-t+1}^{t+1} (-1)^{k-1} \binom{2t}{t-k+1} \Bigg] |k\rangle . \end{aligned} \tag{A4}$$

Let us now collect all terms $-t+1 \leq k \leq t-1$ under the same summation symbol, separating the terms $k = \pm(t+1)$. Equation (A4), using also that:

$$\binom{2t}{0} = \binom{2t}{2t} = 1, \qquad \binom{2t}{1} = \binom{2t}{2t-1} = 2t, \tag{A5}$$

is then rearranged as:

$$\begin{aligned} \hat{H}_\gamma^{t+1} |0\rangle = \gamma^{t+1} \Bigg\{ \sum_{k=-t-1}^{t-1} (-1)^k \left[\binom{2t}{t-k-1} + 2\binom{2t}{t-k} + \binom{2t}{t-k+1} \right] \\ + 4(-1)^t (t+1) - 2(-1)^t \Bigg\} |k\rangle \ . \end{aligned} \tag{A6}$$

Using iteratively the relation:

$$\binom{n}{k} + \binom{n}{k+1} = \binom{n+1}{k+1}, \tag{A7}$$

the sum of binomial coefficients in Equation (A6) can be simplified to a single coefficient, namely:

$$\binom{2t}{t-k-1} + 2\binom{2t}{t-k} + \binom{2t}{t-k+1} = \binom{2(t+1)}{(t+1)-k}. \tag{A8}$$

Next, we observe that the evaluation of the resulting expression under the summation symbol in Equation (A6) for $k = \pm t$ gives the value $2(-1)^t(t+1)$. The evaluation of the same term for $k = \pm(t+1)$ gives $-(-1)^t$ instead. Hence, we can incorporate the last two terms in Equation (A6), $4(-1)^t(t+1) - 2(-1)^t$, into the summation by extending the extrema to $-t-1$ and $t+1$. We finally obtain:

$$\hat{H}_\gamma^{t+1} |0\rangle = \gamma^{t+1} \sum_{k=-t-1}^{t+1} (-1)^k \binom{2(t+1)}{(t+1)-k} |k\rangle \ . \tag{A9}$$

The induction is then complete, and Equation (A1) is proven. Now, to obtain Equation (18), we compute $U(t)|0\rangle$. Therefore, let us start writing the operator as:

$$U(t)|0\rangle = e^{-i\hat{H}_\gamma t}|0\rangle = \sum_{k=0}^{+\infty} \frac{(-i\hat{H}_\gamma t)^k}{k!}|0\rangle = \sum_{k=0}^{+\infty} \frac{(-it)^k}{k!} \left(\gamma^k \sum_{n=-k}^{k} (-1)^n \binom{2k}{k-n} |n\rangle \right), \tag{A10}$$

where we applied the operator $\hat{H}_\gamma$ using the previous result for $\hat{H}_\gamma^{t+1}|0\rangle$. At this point, the two sums can be exchanged by changing the domain. This step is shown in Figure A1, where the red area (vertical lines) represents the original domain and the blue area (horizontal lines) is the new one. As we can see, the two areas are equal because the straight lines, $n = k$ and $n = -k$, split the rectangle into two equal parts. For this reason, we write:

$$\begin{aligned} U(t)|0\rangle &= \sum_{n=-\infty}^{+\infty} \sum_{k=|n|}^{+\infty} \frac{(-i\gamma t)^k}{k!} \overbrace{(-1)^{|n|}}^{e^{i\pi|n|} = e^{i(\frac{\pi}{2}+\frac{\pi}{2})|n|}} \binom{2k}{k-n} |n\rangle \\ &= \sum_{n=-\infty}^{+\infty} e^{i\frac{\pi}{2}|n|} e^{i\frac{\pi}{2}|n|} \sum_{k=|n|}^{+\infty} \frac{(-i\gamma t)^k}{k!} \binom{2k}{k-n} |n\rangle \end{aligned}, \tag{A11}$$

and using the following identity for the Bessel function, which is demonstrated in Appendix B,

$$e^{-2i\gamma t} J_{|n|}(2\gamma t) = e^{i\frac{\pi}{2}|n|} \sum_{k=|n|}^{\infty} \frac{(-i\gamma t)^k}{k!} \binom{2k}{k-n}, \tag{A12}$$

we obtain:

$$U(t)\,|0\rangle = \sum_{n=-\infty}^{+\infty} e^{\mathrm{i}\frac{\pi}{2}|n|-2\mathrm{i}\gamma t} J_{|n|}(2\gamma t)\,|n\rangle = |\psi(t)\rangle\ . \tag{A13}$$

Now, as the last point, we evaluate the probability from the amplitudes Equation (A13):

$$\begin{aligned} P_\gamma(n,t) &= |\langle n|\,U(t)\,|0\rangle|^2 = \\ &= \left|\langle n|\sum_{k=-\infty}^{+\infty} e^{\mathrm{i}\frac{\pi}{2}|k|-2\mathrm{i}\gamma t} J_{|k|}(2\gamma t)\,|k\rangle\right|^2 = \\ &= \left|\sum_{k=-\infty}^{+\infty} e^{\mathrm{i}\frac{\pi}{2}|k|-2\mathrm{i}\gamma t} J_{|k|}(2\gamma t)\,\langle n|k\rangle\right|^2 = \\ &= \left|e^{\mathrm{i}\frac{\pi}{2}|n|-2\mathrm{i}\gamma t} J_{|n|}(2\gamma t)\right|^2 = |J_n(2\gamma t)|^2\ . \end{aligned} \tag{A14}$$

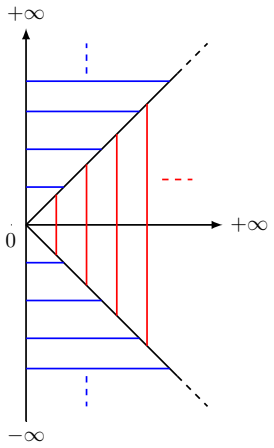

Figure A1. Domain of the sums. Horizontal lines represent the new area, while the vertical ones the original domain.

Appendix B. Bessel Identity Check

Let us consider the case $n > 0$, so the goal is to show that:

$$e^{-2\mathrm{i}\gamma t} J_n(2\gamma t) = e^{\frac{\mathrm{i}\pi n}{2}} \sum_{k=n}^{\infty} \frac{(-\mathrm{i}\gamma t)^k}{k!} \binom{2k}{k-n}. \tag{A15}$$

By changing index k to $\ell = k - n$, we obtain:

$$\frac{e^{-2\mathrm{i}\gamma t} J_n(2\gamma t)}{e^{\frac{\mathrm{i}\pi n}{2}}} = \sum_{\ell=0}^{\infty} \frac{(-\mathrm{i}\gamma t)^\ell}{\ell!} \binom{2(\ell+n)}{\ell} \frac{\ell!}{(\ell+n)!} (-\mathrm{i}\gamma t)^n. \tag{A16}$$

Now, let us change t to $t' = -\mathrm{i}\gamma t$, so we have:

$$\frac{e^{2t'} J_n(2\mathrm{i}t')}{t'^n e^{\frac{\mathrm{i}\pi n}{2}}} = \sum_{\ell=0}^{\infty} \binom{2(\ell+n)}{\ell} \frac{\ell!}{(\ell+n)!} \frac{t'^\ell}{\ell!}. \tag{A17}$$

The right part is the Taylor expansion of the left term, so now, the goal is to show that:

$$e^{-\frac{\mathrm{i}\pi n}{2}} \frac{\mathrm{d}^\ell}{\mathrm{d}t'^\ell} \left(\frac{e^{2t'} J_n(2\mathrm{i}t')}{t'^n}\right)\Bigg|_{t'=0} = \frac{\ell!}{(\ell+n)!} \binom{2(\ell+n)}{\ell}, \tag{A18}$$

by using the well known expression of the Bessel function:

$$J_n(2\mathrm{i}t') = \sum_{m=0}^{\infty} \frac{(-1)^m}{m!(m+n)!}(\mathrm{i}t')^{2m+n} \tag{A19}$$

and the Taylor expansion of the exponential function, $e^{2t'} = \sum_{p=0}^{\infty} \frac{(2t')^p}{p!}$. Thus, we get:

$$\begin{aligned} & e^{-\mathrm{i}\frac{\pi}{2}n} \frac{\mathrm{d}^\ell}{\mathrm{d}t'^\ell} \left(\frac{1}{t'^n} \sum_{p=0}^{\infty} \frac{2^p t'^p}{p!} \sum_{m=0}^{\infty} \frac{(-1)^m \mathrm{i}^{2m+n}}{m!(m+n)!} t'^n t'^{2m} \right) \Big|_{t'=0} \\ & = \sum_{m,p=0}^{\infty} \frac{(-1)^m \mathrm{i}^{2m+n}}{m!(m+n)!} \frac{2^p}{p!} \frac{\mathrm{d}^\ell}{\mathrm{d}t'^\ell} \left(t'^{2m+p} \right) e^{-\mathrm{i}\frac{\pi}{2}n} \Big|_{t'=0}. \end{aligned} \tag{A20}$$

Since we are going to take $t' = 0$, the only terms we have to consider are those such that $2m + p = \ell$. Then:

$$\frac{\mathrm{d}^\ell}{\mathrm{d}t'^\ell} \left(t'^{2m+p} \right) \Big|_{t'=0} = \ell! \qquad \text{and} \qquad 2m + p = \ell \tag{A21}$$

Finally, we have:

$$e^{-\mathrm{i}\frac{\pi}{2}n} \frac{\mathrm{d}^\ell}{\mathrm{d}t'^\ell} \left(\frac{e^{2t'} J_n(2\mathrm{i}t')}{t'^n} \right) \Big|_{t'=0} = \sum_{m=0}^{\infty} \frac{(-1)^m \mathrm{i}^{2m+n} 2^{\ell-2m} \ell!}{m!(m+n)!(\ell-2m)!} e^{-\mathrm{i}\frac{\pi}{2}n}, \tag{A22}$$

$$= \ell! \sum_{m=0}^{\lfloor \frac{\ell}{2} \rfloor} \frac{2^{\ell-2m}}{m!(m+n)!(\ell-2m)!}, \tag{A23}$$

where we have used the fact that $(-1)^m i^{2m+n} e^{-i\frac{\pi}{2}n} = 1$ and m must be at most $\lfloor \frac{\ell}{2} \rfloor$, $\lfloor \cdot \rfloor$ being the floor function, because the argument of the factorial must be greater than or equal to zero. Thus:

$$e^{-\mathrm{i}\frac{\pi}{2}n} \frac{\mathrm{d}^\ell}{\mathrm{d}t'^\ell} \left(\frac{e^{2t'} J_n(2\mathrm{i}t')}{t'^n} \right) \Big|_{t'=0} = \frac{\ell!}{(n+\ell)!} \sum_{m=0}^{\lfloor \frac{\ell}{2} \rfloor} \binom{n+\ell}{m} \binom{n+\ell-m}{\ell-2m} 2^{\ell-2m} \tag{A24}$$

$$= \frac{\ell!}{(n+\ell)!} \binom{2(n+\ell)}{\ell}. \tag{A25}$$

The right term of this last equation is equal to the right term of Equation (A18). In the last step, we used the identity that we will prove in the following Appendix.

Appendix C. Modified Vandermonde's Identity

In Equation (A23), we used a modified version of Vandermonde's identity:

$$\sum_{m=0}^{\lfloor \frac{\ell}{2} \rfloor} \binom{n}{m} \binom{n-m}{\ell-2m} 2^{\ell-2m} = \binom{2n}{\ell}. \tag{A26}$$

It can be proven in many ways, but we will show the combinatorial one. The right part is quite intuitive since it represents the number of subsets of size ℓ in a set of $2n$ elements.

Now, we will show a different way to count the subsets of size ℓ, which correspond to the left hand side. Therefore, let us consider the binary sets defined as $A_i = \{2i-1, 2i\}$ for $i = 1, 2, \ldots, n$ such that we can partition the entire set of size $2n$, $\{1, 2, \ldots, 2n\}$. Now, let us define S as the set of subsets of size ℓ from the set $\{1, 2, \ldots, 2n\}(\{1, 2, \ldots, \ell-1, \ell\}; \{1, 2, \ldots, \ell-1, \ell+1\}; \ldots)$. We can build any set in S by choosing first m sets A_i from the n for which $|S \cap A_i| = 2$. This choice can be done in $\binom{n}{m}$ possible ways. Then, fixing A_i, we choose $\ell - 2m$ sets from the remaining $n - m$, for which $|S \cap A_i| = 1$, and we

have $\binom{n-m}{\ell-2m}$ ways to perform the choice. Moreover, for this last choice, we have $2^{\ell-2m}$ other possible combinations since we are using sets of two elements. Now, summing over all the possible values of m, we get the total number of subsets of size ℓ.

For illustration purposes, we consider now the following example: a set of six elements $\{1,2,3,4,5,6\}$, so $n = 3$, and suppose we have $\ell = 3$. There are $\binom{2n}{\ell} = \binom{6}{3} = 20$ subsets of size three. Alternatively, let us consider the subsets $S = \{1,2,3\}, \{1,2,4\}, \{1,2,5\} \ldots$. To build any set in S, we choose first the set of i such that $|S \cap A_i| = 2$ (i.e., $|S \cap A_1| = |\{1,2\}| = 2, |S \cap A_2| = |\{3,4\}| = 2, |S \cap A_3| = |\{5,6\}| = 2$), which can be done in $\binom{3}{1} = 3$ ways. Then, fixing A_i, we choose from the remaining A_i's those such that $|S \cap A_i| = 1$ (e.g., fixed A_1; we can choose A_2 or A_3 in order to have $|S \cap A_2| = |\{3\}| = 1$ or $|S \cap A_2| = |\{4\}| = 1$ or $|S \cap A_3| = |\{5\}| = 1 \ldots$). This last choice can be done in $2^{\ell-2m}$ possible ways since we are using an alphabet of two elements. In terms of sets A_i we have: $A_1 A_2^+, A_1 A_2^-, A_1^- A_2^- A_3^-, A_1^- A_2^- A_3^+, \ldots$, where $A_i^\pm$ means the even or odd element in A_i. Therefore, in the sum, the first binomial takes into account the number of intersection, with the set S, with two elements; the second binomial represents the number of intersection with one element; and $2^{\ell-2m}$ takes into account the parity of the set A_i. Putting the above reasoning into a formula, we obtain:

$$\sum_{m=0}^{1} \binom{3}{m}\binom{3-m}{3-2m} 2^{3-2m} = \binom{3}{0}\binom{3}{3}2^3 + \binom{3}{1}\binom{2}{1}2^1 = 8 + 12 = 20\,. \tag{A27}$$

References

1. Aharonov, Y.; Davidovich, L.; Zagury, N. Quantum random walks. *Phys. Rev. A* **1993**, *48*, 1687. [CrossRef]
2. Sadgrove, M.; Horikoshi, M.; Sekimura, T.; Nakagawa, K. Rectified Momentum Transport for a Kicked Bose-Einstein Condensate. *Phys. Rev. Lett.* **2007**, *99*, 043002. [CrossRef]
3. Dana, I.; Ramareddy, V.; Talukdar, I.; Summy, G.S. Experimental Realization of Quantum-Resonance Ratchets at Arbitrary Quasimomenta. *Phys. Rev. Lett.* **2008**, *100*, 024103. [CrossRef] [PubMed]
4. White, D.H.; Ruddell, S.K.; Hoogerland, M.D. Experimental realization of a quantum ratchet through phase modulation. *Phys. Rev. A* **2013**, *88*, 063603. [CrossRef]
5. Ni, J.; Dadras, S.; Lam, W.K.; Shrestha, R.K.; Sadgrove, M.; Wimberger, S.; Summy, G.S. Hamiltonian Ratchets with Ultra-Cold Atoms. *Ann. Phys.* **2017**, *529*, 1600335. [CrossRef]
6. Sadgrove, M.; Wimberger, S. A pseudoclassical method for the atom-optics kicked rotor: From theory to experiment and back. In *Advances in Atomic, Molecular, and Optical Physics*; Elsevier: Amsterdam, The Netherlands, 2011; Volume 60, pp. 315–369.
7. Ni, J.; Lam, W.K.; Dadras, S.; Borunda, M.F.; Wimberger, S.; Summy, G.S. Initial-state dependence of a quantum resonance ratchet. *Phys. Rev. A* **2016**, *94*, 043620. [CrossRef]
8. Portugal, R. *Quantum Walks and Search Algorithms*; Springer: Berlin, Germany, 2013.
9. Delvecchio, M.; Groiseau, C.; Petiziol, F.; Summy, G.; Wimberger, S. Quantum search with a continuous-time quantum walk in momentum space. *J. Phys. B* **2019**, in press. [CrossRef]
10. Bouwmeester, D.; Marzoli, I.; Karman, G.P.; Schleich, W.; Woerdman, J.P. Optical Galton board. *Phys. Rev. A* **1999**, *61*, 013410. [CrossRef]
11. Du, J.; Li, H.; Xu, X.; Shi, M.; Wu, J.; Zhou, X.; Han, R. Experimental implementation of the quantum random-walk algorithm. *Phys. Rev. A* **2003**, *67*, 042316. [CrossRef]
12. Perets, H.B.; Lahini, Y.; Pozzi, F.; Sorel, M.; Morandotti, R.; Silberberg, Y. Realization of quantum walks with negligible decoherence in waveguide lattices. *Phys. Rev. Lett.* **2008**, *100*, 170506. [CrossRef]
13. Tang, H.; Lin, X.F.; Feng, Z.; Chen, J.Y.; Gao, J.; Sun, K.; Wang, C.Y.; Lai, P.C.; Xu, X.Y.; Wang, Y.; et al. Experimental two-dimensional quantum walk on a photonic chip. *Sci. Adv.* **2018**, *4*. [CrossRef] [PubMed]
14. Izaac, J.A.; Zhan, X.; Bian, Z.; Wang, K.; Li, J.; Wang, J.B.; Xue, P. Centrality measure based on continuous-time quantum walks and experimental realization. *Phys. Rev. A* **2017**, *95*, 032318. [CrossRef]
15. Preiss, P.M.; Ma, R.; Tai, M.E.; Lukin, A.; Rispoli, M.; Zupancic, P.; Lahini, Y.; Islam, R.; Greiner, M. Strongly correlated quantum walks in optical lattices. *Science* **2015**, *347*, 1229–1233. [CrossRef] [PubMed]

16. Summy, G.; Wimberger, S. Quantum random walk of a Bose-Einstein condensate in momentum space. *Phys. Rev. A* **2016**, *93*, 023638.
17. Weiß, M.; Groiseau, C.; Lam, W.K.; Burioni, R.; Vezzani, A.; Summy, G.S.; Wimberger, S. Steering random walks with kicked ultracold atoms. *Phys. Rev. A* **2015**, *92*, 033606. [CrossRef]
18. Dadras, S.; Gresch, A.; Groiseau, C.; Wimberger, S.; Summy, G.S. Quantum Walk in Momentum Space with a Bose-Einstein Condensate. *Phys. Rev. Lett.* **2018**, *121*, 070402. [CrossRef]
19. Dadras, S.; Gresch, A.; Groiseau, C.; Wimberger, S.; Summy, G.S. Experimental realization of a momentum-space quantum walk. *Phys. Rev. A* **2019**, *99*, 043617. [CrossRef]
20. Knight, P.L.; Roldán, E.; Sipe, J.E. Quantum walk on the line as an interference phenomenon. *Phys. Rev. A* **2003**, *68*, 020301. [CrossRef]
21. Buerschaper, O.; Burnett, K. Stroboscopic quantum walks. *arXiv* **2004**, arXiv: quant-ph/0406039.
22. Ishkhanyan, A.M. Narrowing of interference fringes in diffraction of prepared atoms by standing waves. *Phys. Rev. A* **2000**, *61*, 063609. [CrossRef]
23. Romanelli, A.; Hernández, G. Anomalous diffusion in the resonant quantum kicked rotor. *Phys. A Stat. Mech. Appl.* **2010**, *389*, 3420–3426. [CrossRef]
24. Hernández, G.; Romanelli, A. Resonant quantum kicked rotor with two internal levels. *Phys. Rev. A* **2013**, *87*, 042316. [CrossRef]
25. Romanelli, A.; Hernández, G. Driving the resonant quantum kicked rotor via extended initial conditions. *Eur. Phys. J. D* **2011**, *64*, 131–136. [CrossRef]
26. Matsuoka, L.; Segawa, E.; Yuki, K.; Konno, N.; Obata, N. Asymptotic behavior of a rotational population distribution in a molecular quantum-kicked rotor with ideal quantum resonance. *Phys. Lett. A* **2017**, *381*, 1773–1779. [CrossRef]
27. Matsuoka, L. Unified parameter for localization in isotope-selective rotational excitation of diatomic molecules using a train of optical pulses. *Phys. Rev. A* **2015**, *91*, 043420. [CrossRef]
28. Behinaein, G.; Ramareddy, V.; Ahmadi, P.; Summy, G.S. Exploring the Phase Space of the Quantum δ-Kicked Accelerator. *Phys. Rev. Lett.* **2006**, *97*, 244101. [CrossRef]
29. Casati, G.; Chirikov, B.; Ford, J.; Izrailev, F. Stochastic Behavior of A Quantum Pendulum Under Periodic Perturbation. In *Lecture Notes in Physics*; Casati, G., Ford, J., Eds.; Springer: Berlin, Germany, 1979.
30. Fishman, S. Quantum Localization. In *Quantum Chaos*; Casati, G., Chirikov, B.V., eds.; School "E. Fermi" CXIX; IOS – North Holland: Amsterdam, The Netherlands, 1993.
31. Wimberger, S. *Nonlinear Dynamics and Quantum Chaos*; Springer: Cham, Switzerland, 2014.
32. Izrailev, F.M. Simple models of quantum chaos: Spectrum and eigenfunctions. *Phys. Rep.* **1990**, *196*, 299–392. [CrossRef]
33. Raizen, M.G. Quantum chaos with cold atoms. *Adv. Atom Molec. Opt. Phys.* **1999**, *41*, 199.
34. Duffy, G.J.; Parkins, S.; Müller, T.; Sadgrove, M.; Leonhardt, R.; Wilson, A.C. Experimental investigation of early-time diffusion in the quantum kicked rotor using a Bose-Einstein condensate. *Phys. Rev. E* **2004**, *70*, 056206. [CrossRef]
35. Ryu, C.; Andersen, M.F.; Vaziri, A.; d'Arcy, M.B.; Grossman, J.M.; Helmerson, K.; Phillips, W.D. High-Order Quantum Resonances Observed in a Periodically Kicked Bose-Einstein Condensate. *Phys. Rev. Lett.* **2006**, *96*, 160403. [CrossRef]
36. Wimberger, S.; Guarneri, I.; Fishman, S. Quantum resonances and decoherence for delta-kicked atoms. *Nonlinearity* **2003**, *16*, 1381. [CrossRef]
37. Abramowitz, M.; Stegun, I.A. *Handbook of Mathematical Functions*; Dover: New York, NY, USA, 1972.
38. Farhi, E.; Gutmann, S. Quantum computation and decision trees. *Phys. Rev. A* **1998**, *58*, 915–928. [CrossRef]
39. Sadgrove, M.; Wimberger, S.; Nakagawa, K. Phase-selected momentum transport in ultra-cold atoms. *Eur. Phys. J. D* **2012**, *66*, 155. [CrossRef]
40. Alberti, A.; Wimberger, S. Quantum walk of a Bose-Einstein condensate in the Brillouin zone. *Phys. Rev. A* **2017**, *96*, 023620. [CrossRef]
41. Ho, D.Y.H.; Gong, J. Quantized Adiabatic Transport In Momentum Space. *Phys. Rev. Lett.* **2012**, *109*, 010601. [CrossRef]
42. Chen, Y.; Tian, C. Planck's Quantum-Driven Integer Quantum Hall Effect in Chaos. *Phys. Rev. Lett.* **2014**, *113*, 216802. [CrossRef]

43. Dana, I. Topological properties of adiabatically varied Floquet systems. *Phys. Rev. E* **2017**, *96*, 022216. [CrossRef]
44. Zhou, L.; Gong, J. Floquet topological phases in a spin-1/2 double kicked rotor. *Phys. Rev. A* **2018**, *97*, 063603. [CrossRef]
45. Groiseau, C.; Wagner, A.; Summy, G.S.; Wimberger, S. Impact of Lattice Vibrations on the Dynamics of a Spinor Atom-Optics Kicked Rotor. *Condens. Matter* **2019**, *4*, 10. [CrossRef]